Geophysical Journal International

Geophys. J. Int. (2016) **205,** 1804–1812
Advance Access publication 2016 March 30
GJI Gravity, geodesy and tides

doi: 10.1093/gji/ggw115

On computing the geoelastic response to a disk load

M. Bevis,[1] D. Melini[2] and G. Spada[3]

[1]*School of Earth Sciences, the Ohio State University, Columbus, Ohio, USA*
[2]*Istituto Nazionale di Geofisica e Vulcanologia, Via di Vigna Murata* 605, *I*-00143 *Rome, Italy*
[3]*Dipartimento di Scienze Pure e Applicate (DiSPeA), Università di Urbino, Italy. E-mail: giorgio.spada@gmail.com*

Accepted 2016 March 24. Received 2016 March 24; in original form 2015 December 18

SUMMARY

We review the theory of the Earth's elastic and gravitational response to a surface disk load. The solutions for displacement of the surface and the geoid are developed using expansions of Legendre polynomials, their derivatives and the load Love numbers. We provide a MATLAB function called `diskload` that computes the solutions for both uncompensated and compensated disk loads. In order to numerically implement the Legendre expansions, it is necessary to choose a harmonic degree, $n_{\max}$, at which to truncate the series used to construct the solutions. We present a rule of thumb (ROT) for choosing an appropriate value of $n_{\max}$, describe the consequences of truncating the expansions prematurely and provide a means to judiciously violate the ROT when that becomes a practical necessity.

Key words: Numerical approximations and analysis; Global change from geodesy; Geomechanics; Mechanics, theory, and modelling.

1 INTRODUCTION

The problem of computing the deformations of an elastic body subject to surface loads has a very long history involving many illustrious mathematicians and physicists (Boussinesq 1885; Lamb 1901; Love 1911, 1929; Shida 1912; Terazawa 1916; Munk & MacDonald 1960; Longman 1962, 1963; Farrell 1972). The easily-coded solution for a uniform elastic half-space (Becker & Bevis 2004) is useful in many engineering contexts, but it is often inappropriate for geophysical applications, since the Earth is neither a half-space nor homogeneous. The solution for a layered elastic half-space (e.g. Pan *et al.* 2007) has wider applicability, but even this formalism is inappropriate for loads with large apertures, or to compute deformations at large distances from the load, where large refers to a significant fraction of the Earth's radius, or greater. Therefore, the preferred framework for most geophysical applications is that of a layered, elastic, self-gravitating sphere with a fluid core (Farrell 1972). The solution for this problem is nearly always developed in terms of expansions involving the load Love numbers, often represented using the symbols (h'_n, k'_n, l'_n), or just (h_n, k_n, l_n) when the loading context is clear. Typically, these treatments invoke either point loads or disk loads.

The point load formalism is often invalid close to the nominal point load, and in that sense the disk load formalism is more flexible. We note that the Love number formalism is appropriate for spherically symmetric elastic Earth models; transverse anisotropy can be incorporated in this class of models as long as it honours spherical symmetry (Pan *et al.* 2015). General classes of elastic anisotropy (e.g. laterally varying transverse and azimuthal anisotropy) break spherical symmetry, in which case the Love number approach is no longer appropriate, and different approaches such as self-gravitating finite element models are needed (though they present their own computational difficulties). Anyone using the equations and the code presented in this paper is implicitly assuming that elastic anisotropy is either absent or of a very special kind.

Between 1975 and 2000, most of the geophysical literature on the surface loading problem focused on glacial isostatic adjustment which addresses the loading response of a viscoelastic Earth (Haskell 1935; Cathles 1975; Peltier & Andrews 1976; Wu & Peltier 1982). Nearly all of these studies also use a Love number formulation. The linear elastic and linear viscoelastic versions of the loading problem are connected via the elastic-viscoelastic correspondence principle (Alfrey 1944; Read 1950; Lee 1950). But, beginning in 2001, there has been a major resurgence of interest in the purely elastic problem. This is because (i) geodesists and geophysicists began to realize that networks of Global Positioning System (GPS) receivers, and more recently Global Navigation Satellite System (GNSS) receivers, were recording seasonal, sustained (i.e. progressive) and transient elastic displacements driven by contemporary changes in the loads imposed on the solid Earth by water, snow and ice (Blewitt *et al.* 2001; Heki 2001; Mangiarotti *et al.* 2001; Dong *et al.* 2002; Bevis *et al.* 2005) and, to a lesser extent, by atmospheric pressure variations (Vandam *et al.* 1994), and (ii) geodetic observations of the Earth's elastic deformation could be used to monitor changes in ice mass (Khan *et al.* 2010; Bevis *et al.* 2012; Nielsen *et al.* 2012; Spada *et al.* 2012; Nielsen *et al.* 2013) and in terrestrial water storage (Bevis *et al.* 2004, 2005; Steckler *et al.* 2010; Fu *et al.* 2013; Borsa *et al.* 2014), and so provide a new means to study climate cycles and climate change.

The easiest way to characterize a distributed load or load change is to represent it as one or more, often many more disk loads. If mass or mass change fields are represented as grids, then each grid cell

can be treated as a disk load or, should it reside in the far-field of the geodetic station, as a point load. The response to a point load can be equated with that of a small and remote disk load, except very close to the point load where the point load concept itself is almost never realistic. Our purposes in this paper are two-fold. First, we wish to provide non-specialists with a simple but complete discussion of how to compute the Earth's elastic response to a disk load. We provide a MATLAB function (`diskload`) that implements this algorithm. Our code, like nearly all of its cousins, sums terms consisting of load Love numbers and Legendre polynomials, or derivatives of Legendre polynomials, all of degree $n = 0, 1, 2, \ldots n_{\max}$. It is important to choose an appropriate value for $n_{\max}$, especially when we seek accurate estimates of the near-field response to the load. Second, we explain how do this, and examine the consequences of prematurely truncating the expansion, that is, choosing or setting $n_{\max}$ too low. This mistake is quite easily made when modelling the elastic response of geodetic stations located close to the edge of ice sheets whose mass losses are being characterized with very high resolution digital elevation models (DEMs), since the appropriate value for $n_{\max}$ increases inversely with the grid spacing or cell size of the DEM. We hope that this discussion will help our readers use more general and complex software packages, such as `REAR` (Melini *et al.* 2015a,b) with increased confidence.

2 THEORY

The so-called 'disk load' is a particular type of surface mass density distribution, characterized by a (i) uniform imposed pressure, that is, constant load 'thickness', and (ii) axial symmetry, two features that make the disk load very handy in applications related to glacial isostasy (e.g. Spada *et al.* 2012; Melini *et al.* 2015b) because of its straightforward expansion in a series of spherical harmonic functions. The disk load can be defined in several ways, which differ in how the problem of mass conservation is addressed (Spada 1993).

The first and more intuitive definition is

$$\sigma(\vartheta) = \rho \begin{cases} T, & 0 \le \vartheta \le \alpha \\ 0, & \text{elsewhere}, \end{cases} \tag{1}$$

where ϑ is colatitude in a local reference frame where the z axis is the axis of symmetry of the load ($0 \le \vartheta \le \pi$), the load function $\sigma(\vartheta)$ has units of mass per unit surface, α defines the load margin where $\sigma(\vartheta)$ is discontinuous, and T represents the (constant) load thickness expressed as the height or depth of an equivalent water load. The point where $\vartheta = 0$ defines the pole of the disk load. In (1), ρ is the load mass density. Using basic formulae in spherical trigonometry and exploiting the spherical symmetry of the Earth model and the axial symmetry of the disk load, it is always possible to transform the load-induced surface displacements from the local to the geographical reference frame (e.g. Melini *et al.* 2015b).

A major problem with definition (1) is that it violates the principle of mass conservation. The mass associated with the disk load

$$M_{\text{disk}} = R_e^2 \int_\Omega \sigma(\vartheta)\, \sin\vartheta \, \mathrm{d}\vartheta, \tag{2}$$

where Ω is the Earth's surface and R_e is its radius, is $M_{\text{disk}} = 2\pi\, \rho\, R_e^2\, T\, (1 - \cos\alpha) \neq 0$. For this reason, we call the load described by eq. (1) an *uncompensated* disk load. In order to conserve mass globally, some compensating load has to be introduced and this can be achieved in many ways, for example by invoking loads of arbitrary shape but appropriate total mass. However, using only disk loads, mass conservation can only be achieved in just two ways.

One possibility is to assume that the compensating mass change is evenly distributed everywhere outside the loading cell defined by (1), a strategy that is suitable when the location of the compensating mass is not exactly known. The geometry of this situation is illustrated in Fig. 1(a). The advantage of this approach is that no extra parameters are required to define the load function $\sigma(\vartheta)$, which preserves its axial symmetry; the disadvantage is the inaccuracy of the load geometry. This disk load has the form

$$\sigma(\vartheta) = \rho \begin{cases} T, & 0 \le \vartheta \le \alpha \\ T', & \text{elsewhere}, \end{cases} \tag{3}$$

where the load defined on the top line is the same as in eq. (1), and the compensating load at the bottom line ensures mass conservation, given an appropriate choice for T' (Spada 1993), that is,

$$\sigma(\vartheta) = \rho \begin{cases} T, & 0 \le \vartheta \le \alpha \\ -\left(\dfrac{1-\cos\alpha}{1+\cos\alpha}\right) T, & \text{elsewhere}, \end{cases} \tag{4}$$

which will be referred to as *compensated* disk load, for which $M_{\text{disk}} = 0$. We note that the term in parentheses in the second line of eq. (4) represents the ratio of the areas of load and compensation.

Alternatively, if one invokes an uncompensated disk load, mass can be still be conserved by introducing one or more additional uncompensated disk loads such that their total mass is zero. This approach is illustrated in Fig. 1(b). In this case mass conservation is accomplished on the basis of some specific geophysical intuition. For example, if the primary disk load represents an ice cap, the compensating ones could be distributed over the oceans to fit the shape of the coastlines. The number of free parameters would increase, but this will be accompanied by an increased accuracy of the global load (note that such a distribution of disks would, unavoidably, contain interstices or overlaps). Again, exploiting the symmetry of each individual disk load and using the superposition principle, the problem can be reduced to the computation of the Earth's response to one single uncompensated disk load, which enormously facilitates the numerical applications (e.g. Spada *et al.* 2012; Melini *et al.* 2015b).

In order to apply the Love number formalism to the disk loading problem (e.g. Spada *et al.* 2011), it is convenient to expand the load in a series of Legendre polynomials

$$\sigma(\vartheta) = \sum_{n=0}^{n_{\max}} \sigma_n P_n(\cos\vartheta), \tag{5}$$

where $\sigma(\vartheta)$ is the load function corresponding to a compensated or an uncompensated load, $P_n(\cos\vartheta)$ is the Legendre polynomial of degree n and the maximum harmonic degree of the expansion $n_{\max}$ plays an important role (Section 4). By the orthogonality of Legendre polynomials, the coefficients of the expansion (5) are

$$\sigma_n = \frac{2n+1}{2} \int_0^\pi \sigma(\vartheta) P_n(\cos\vartheta) \sin\vartheta \, \mathrm{d}\vartheta \quad (n = 0, 1, \ldots n_{\max}). \tag{6}$$

Since both uncompensated and compensated disk loads are described in terms of piecewise constant functions (see eqs 1 and 4), this integral can be easily evaluated in closed form, taking into account the property of Legendre polynomials $P_n(z) = \frac{P'_{n+1}(z) - P'_{n-1}(z)}{2n+1}$, where $z \equiv \cos\vartheta$ and $P'_n(z) \equiv \frac{\mathrm{d}P_n}{\mathrm{d}z}$.

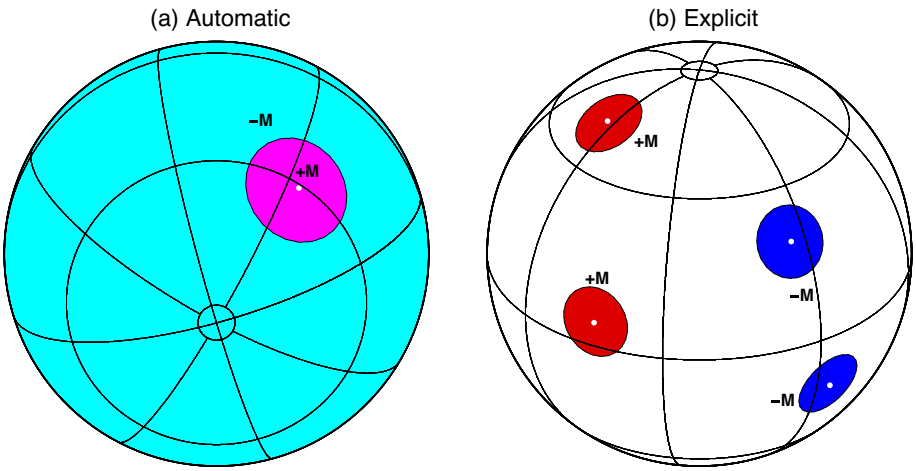

Figure 1. Two ways of conserving the total mass of the load. In panel (a), the disk load of mass $+M = M_{\rm disk}$ (magenta) is automatically compensated by a complementary load of mass $-M$ (cyan) according to eq. (4). In panel (b), several disk loads like (1) are explicitly used (red) and compensated by disks of mass $-M$ (blue), with a vanishing total mass. Small white circles mark the poles of the disk loads.

For the *uncompensated* disk load (1), the expansion coefficients are

$$\sigma_n = \frac{\rho T}{2} \begin{cases} (1-\cos\alpha) & n=0 \\ -P_{n+1}(\cos\alpha) + P_{n-1}(\cos\alpha) & n \geq 1, \end{cases} \tag{7}$$

whereas for the *compensated* load (4), they are

$$\sigma_n = \rho T \begin{cases} 0 & n=0 \\ -\dfrac{P_{n+1}(\cos\alpha) - P_{n-1}(\cos\alpha)}{1+\cos\alpha} & n \geq 1, \end{cases} \tag{8}$$

where conditions $\sigma_0 \neq 0$ in eq. (7) and $\sigma_0 = 0$ in eq. (8) reflect the violation and the observance of mass conservation, respectively. In the limit of small loads (i.e. for $\alpha \to 0$), eq. (7) reduces to eq. (8), showing that the mass conservation constraint becomes increasingly important with increasing disk size. We note that, for $n \neq 0$, the ratio of eqs (7) to (8) is ${}^1/_2(1+\cos\alpha)$, which is not dependent upon n nor T. It is simple to show that the expansion coefficients for the uncompensated and the compensated loads differ by more than 5 per cent only for loads of relatively large size, with $\alpha \gtrsim 25^\circ$.

Exploiting the axial symmetry of the disk loads, and assuming a spherically symmetric Earth, the load-induced displacement $\mathbf{u}$ at any given point P on the Earth's surface will possess a vertical (U) and a horizontal (V) component. In the local reference frame

$$\mathbf{u}(P) = U(\vartheta)\,\hat{\mathbf{r}} + V(\vartheta)\,\hat{\boldsymbol{\vartheta}}, \tag{9}$$

where unit vectors $\hat{\mathbf{r}}$ and $\hat{\boldsymbol{\vartheta}}$ point upwards and in the direction of increasing co-latitude, respectively. Using the general formalism for loading problems in spherical geometry (e.g. Farrell 1972; Spada *et al.* 2011), expressions for $U(\vartheta)$ and $V(\vartheta)$ for axis-symmetric loads are easily obtained. They read:

$$U(\vartheta) = \frac{4\pi R_e^3}{M_e} \sum_{n=0}^{n_{\max}} \frac{\sigma_n\, h_n}{2n+1}\, P_n(\cos\vartheta) \tag{10}$$

and

$$V(\vartheta) = \frac{4\pi R_e^3}{M_e} \sum_{n=1}^{n_{\max}} \frac{\sigma_n\, l_n}{2n+1} \frac{\partial P_n(\cos\vartheta)}{\partial\vartheta}, \tag{11}$$

respectively, where M_e is the Earth's mass, and (h_n, l_n) are the elastic load-deformation coefficients of degree n for vertical and horizontal displacement, respectively (e.g. Farrell 1972). The series in eqs (10) and (11) cannot be summed to obtain closed-form solutions for $U(\vartheta)$ and $V(\vartheta)$ due to the complicated n-dependence of σ_n and (h_n, l_n). However, for a point load, one can take advantage from the so-called Legendre sums in order to decompose the displacements into an analytical and a numerical part (Farrell 1972; Na & Baek 2011). In eq. (10), the sum includes a term of degree $n = 0$ since a compressible elastic Earth can change its radius when subject to a uniform load; however this term is not included in eq. (11) since l_0 vanishes by virtue of the spherical symmetry of the Earth model and of the surface load (Farrell 1972). Both surface loading and induced deformation cause perturbations of geoid height $G(\vartheta)$ which can be obtained by replacing the Love number h_n in (10) with $1 + k_n$, where k_n is the Love number for gravity potential. We note that the '1' in $1 + k_n$ accounts for the direct gravitational effect of the load, whereas k_n accounts for the gravity variations caused by the Earth deformation produced by the load (Farrell 1972). As shown by Longman (1962), $k_0 = 0$. We note that, for a given load size α, $U(\vartheta)$, $V(\vartheta)$ and $G(\vartheta)$ are proportional to T, for both uncompensated and compensated disk loads. This follows directly from the laws of linear elasticity, and it is expressed by eqs (7) and (8), respectively.

We point out that the derivative in eq. (11) can be expressed as a combination of Legendre polynomials. In fact, with $z = \cos\vartheta$, $\frac{\partial P_n(\cos\vartheta)}{\partial\vartheta} = -\sin\vartheta \cdot P_n'(z)$, which can be transformed using recurrence relations for the derivative of the Legendre polynomials (i.e. $\frac{z^2-1}{n} P_n'(z) = z P_n(z) - P_{n-1}(z)$), so as to obtain the following equivalent form for horizontal displacement

$$V(\vartheta) = -\frac{4\pi R_e^3}{M_e} \frac{1}{\sin\vartheta} \sum_{n=1}^{n_{\max}} \frac{n\,\sigma_n\, l_n}{2n+1} \times \left(P_{n-1}(\cos\vartheta) - \cos\vartheta\; P_n(\cos\vartheta)\right). \tag{12}$$

The formulae presented above are implemented in our MATLAB function `diskload` (see Supporting Information Text S1).

3 THE LOAD LOVE NUMBERS

The load Love numbers (h_n, k_n, l_n) depend on the elastic structure of the Earth, so each Earth model is associated with its own set of Love numbers. Computing the Love numbers is considerably more difficult than using them to compute the elastic response to a disk

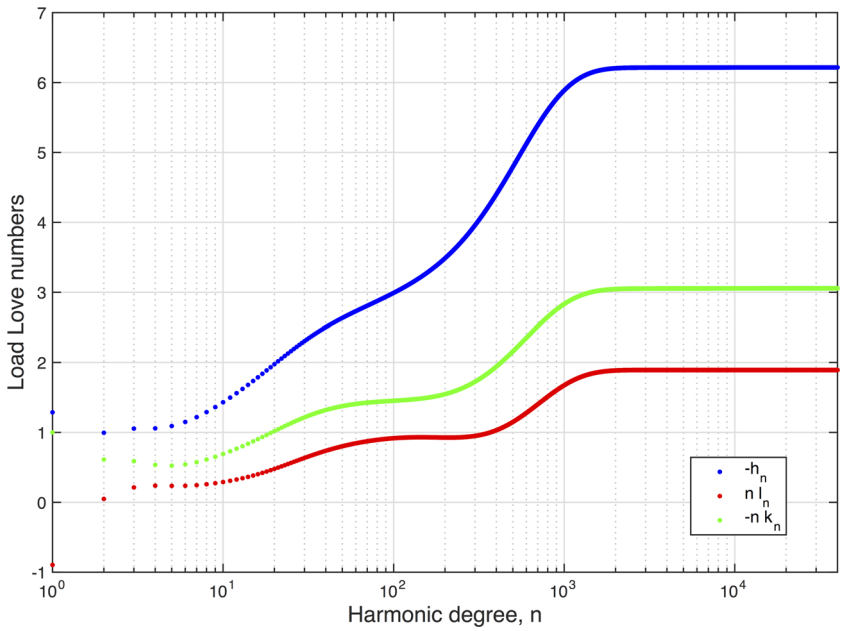

Figure 2. Load Love numbers (h_n, k_n, l_n) for model REF, as a function of harmonic degree n. Note that $h_0 = -0.216$ and $k_0 = l_0 = 0$ are not shown due to the logarithmic scale.

load, and as a result this task is usually left to specialists (see e.g. Pan *et al.* 2015 and references therein). In addition to our MATLAB function `diskload`, we provide the reader with a set of Love numbers associated with the seismological Earth model REF of Kustowski *et al.* (2007). This set of Love numbers, which we use in Section 4, is complete through degree 40 000. Obviously, utilizing this particular set of Love numbers with `diskload` means we can invoke $n_{\max} \leq 40\,000$, but no higher. However, users of `diskload` can use Love numbers associated with other Earth models, and seek out Love number listings that permit higher values of $n_{\max}$. According to our experience, standard Fortran routines (e.g. Press 2007) and the MATLAB function `pLegendre` that comes with diskload can compute reliably the Legendre polynomials to harmonic degrees as high as 10^7. However, possible errors can be associated with the evaluation of high degree Love numbers, unless the computations are performed with sufficient precision (Spada 2008; Spada *et al.* 2011) and possibly with the help of analytical solutions (Grapenthin 2014; Pan *et al.* 2015).

In Fig. 2, the Love numbers for the seismological model REF of Kustowski *et al.* (2007) are shown as a function of the harmonic degree n. The Love numbers are expressed in the reference frame having the origin in the centre of mass of the (Earth+Load) system, which imposes $1 + k_1 = 0$ (Farrell 1972). With a different choice of the reference frame, the value of the three degree $n = 1$ Love numbers would be modified (Spada *et al.* 2011). While the Love number for vertical displacement (h_n) reaches a constant value with increasing n, those for horizontal displacement (l_n) and for the gravitational potential (k_n) decay as $^1/_n$. As pointed out by Farrell (1972), the asymptotic dependence of the Love numbers for large n values matches the solution of the Boussinesq problem, which applies to a flat and homogeneous Earth model (Boussinesq 1885). This shows that with increasing n the Love numbers become increasingly sensitive to the values of the elastic constants of the Earth's outmost layers. This property can be exploited to test the consistency of numerical computation of high-degree Love numbers (Farrell 1972) or to approximately extend a given set of Love numbers to higher harmonic degrees.

4 THE TRUNCATION PROBLEM

We now investigate the problem of choosing an appropriate value for the maximum degree, $n_{\max}$, used in expansions (10) and (12), and to explore the consequences of premature truncation (i.e. choosing $n_{\max}$ too low). As we shall see, the appropriate value of $n_{\max}$ depends on the size of the disk, and also on the accuracy required in the near-field of the load. The dependence on the size of the disk is reasonable given that we expanded the load in eq. (5), and, intuitively, the load will be fairly well represented by this expansion only if it includes wavelengths comparable to, or (better) smaller than the radius of the load. Rather less obvious is that this requirement can be relaxed as we move into the far-field of the disk, where the elastic response becomes indistinguishable from that due to a point load (Farrell 1972), and the geometry of the disk is no longer sensed or relevant. The wavelength, λ, associated with a spherical surface harmonic of degree n is approximately given by Jeans' relation:

$$\lambda \approx \frac{2\pi R_e}{n + {}^1/_2} \tag{13}$$

(Jeans 1923; Dahlen & Tromp 1998), where R_e is the radius of the Earth. Since its circumference $2\pi R_e$ is roughly 40 000 km, the smallest wavelength associated with an expansion through degree $n_{\max} = 40\,000$ is $\lambda_{\min} \approx 1$ km. If a disk has angular radius α, and radius $d = \alpha R_e$, seeking a value of $n_{\max}$ that produces $\lambda_{\min} \lesssim d$ leads to the following rule of thumb (ROT)

$$\text{set} \quad n_{\max} \gtrsim \overline{n}_{\max} = \frac{2\pi R_e}{d} = \frac{360^\circ}{\alpha}, \tag{14}$$

where is α is the radius stated in degrees. Since in almost any geophysical application $n_{\max} \gg 100$, we made the approximation $n + {}^1/_2 \approx n$ in deriving (14). In nearly all applications, setting $n_{\max} = 2\,\overline{n}_{\max}$ is very defensive and easily satisfies the ROT, though, as we point out in Section 5, in applications involving loads modelled using many disks it is nearly always adequate to set $n_{\max} = \overline{n}_{\max}$, and–with care–it may be possible to set $n_{\max} < \overline{n}_{\max}$ and yet do little damage to the solution.

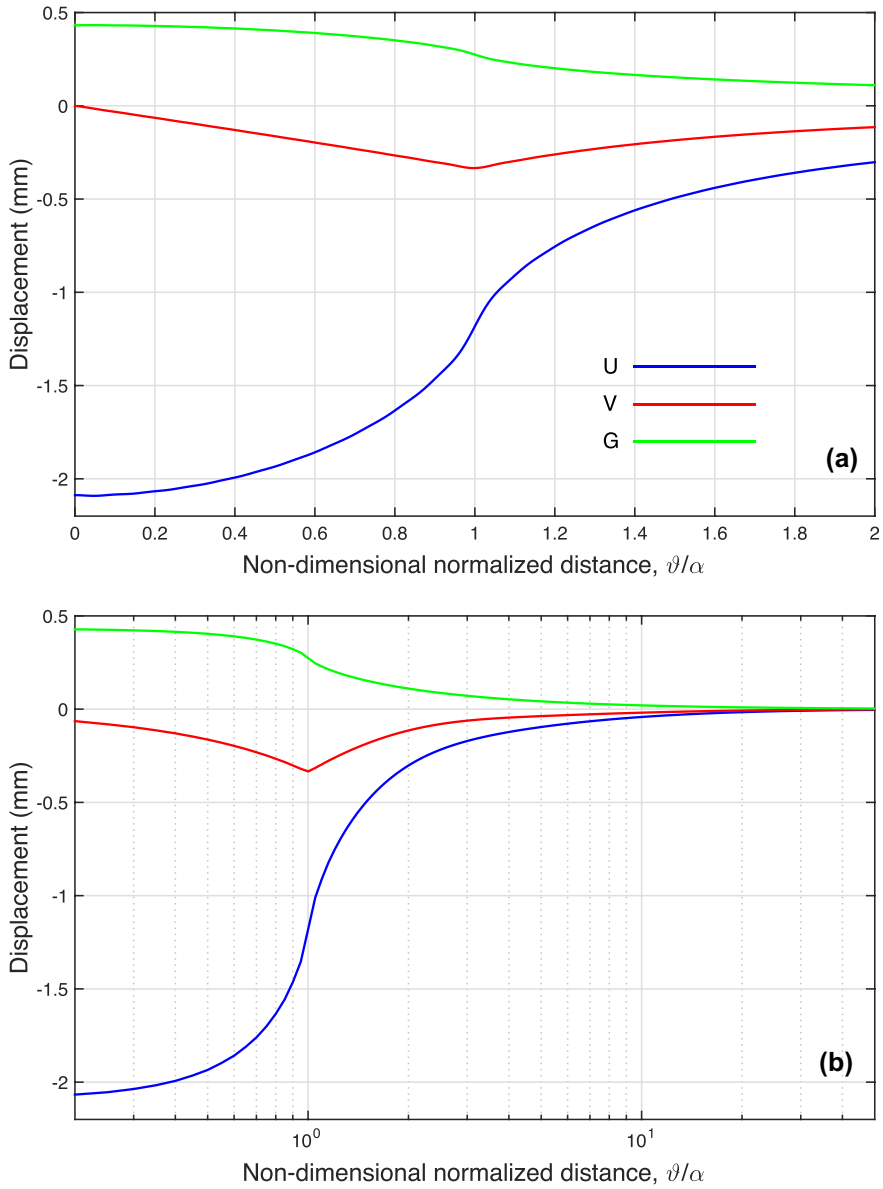

Figure 3. Vertical displacement (U), horizontal displacement (V) and geoid height variation (G) for an ice disk load with $\alpha = 0.1^\circ$ and thickness $T = +1$ m, as a function of ϑ/α, in the near field (a) and in the far field (b). Disk thickness is expressed as equivalent water height corresponding to an ice density $\rho_i = 917$ kg m^{-3}.

We now illustrate the issues pertaining to the ROT using the case of a compensated ice disk load with angular radius $\alpha = 0.1^\circ$ and a thickness of $T = +1$ m. Our ROT requires us to set $n_{\max} \gtrsim \overline{n}_{\max}$ and since $\overline{n}_{\max} = 3600$, for a disk of radius 0.1°, this requirement is easily satisfied if we set $n_{\max} = 40\,000$. Accordingly, we used `diskload`, with $n_{\max}$ set to 40 000, to compute the vertical $U(\vartheta)$ and horizontal $V(\vartheta)$ components of displacement as functions of the angular distance, ϑ, measured from the centre of the disk. We can think of ϑ as colatitude referred to a pole in the centre of the disk. In Fig. 3, we graph U, V and G as functions of the normalized distance ϑ/α, emphasizing the near-field (Fig. 3a) and the far-field (Fig. 3b) responses. We note that effectively the curves always depend on ϑ and α, not ϑ/α, and there is no 'universal' shape to the curves no matter how the plot axes are normalized (see Supporting Information Text S3). The curves in Fig. 3 reproduce, to very high precision, those computed by the program `REAR` (Melini *et al.* 2015a), thereby validating our MATLAB function. Note that the load causes elastic subsidence ($U(\vartheta) < 0$) which attains its extreme value (-2.09 mm) at the centre or pole of the disk, and poleward horizontal displacement ($V(\vartheta) < 0$) which attains its extreme value (-0.33 mm) at the edge of the disk. The amplitude of $V(\vartheta)$ falls to zero at the centre of the disk, as required by the axial symmetry of the load. The amplitudes of both components decrease monotonically with increasing distance from the edge of the load. The geoid height variation $G(\vartheta)$ attains positive values, which denotes an under-compensated load (Spada *et al.* 2011), and it is strongly anti-correlated with $U(\vartheta)$. At the pole of the load, its maximum amplitude is $+0.43$ mm. Maximum values of U, V and G are found to depend linearly on the disk size for small loads, matching the scaling laws that hold for the flat and homogeneous Earth model (see Supporting Information Text S3; Boussinesq 1885; Lamb 1901; Terazawa 1916).

We now consider, in Fig. 4, what happens when we set $n_{\max} \approx \overline{n}_{\max}$ or if we truncate the expansions prematurely by setting either $n_{\max} < \overline{n}_{\max}$ or $n_{\max} \ll \overline{n}_{\max}$. We define the numerical

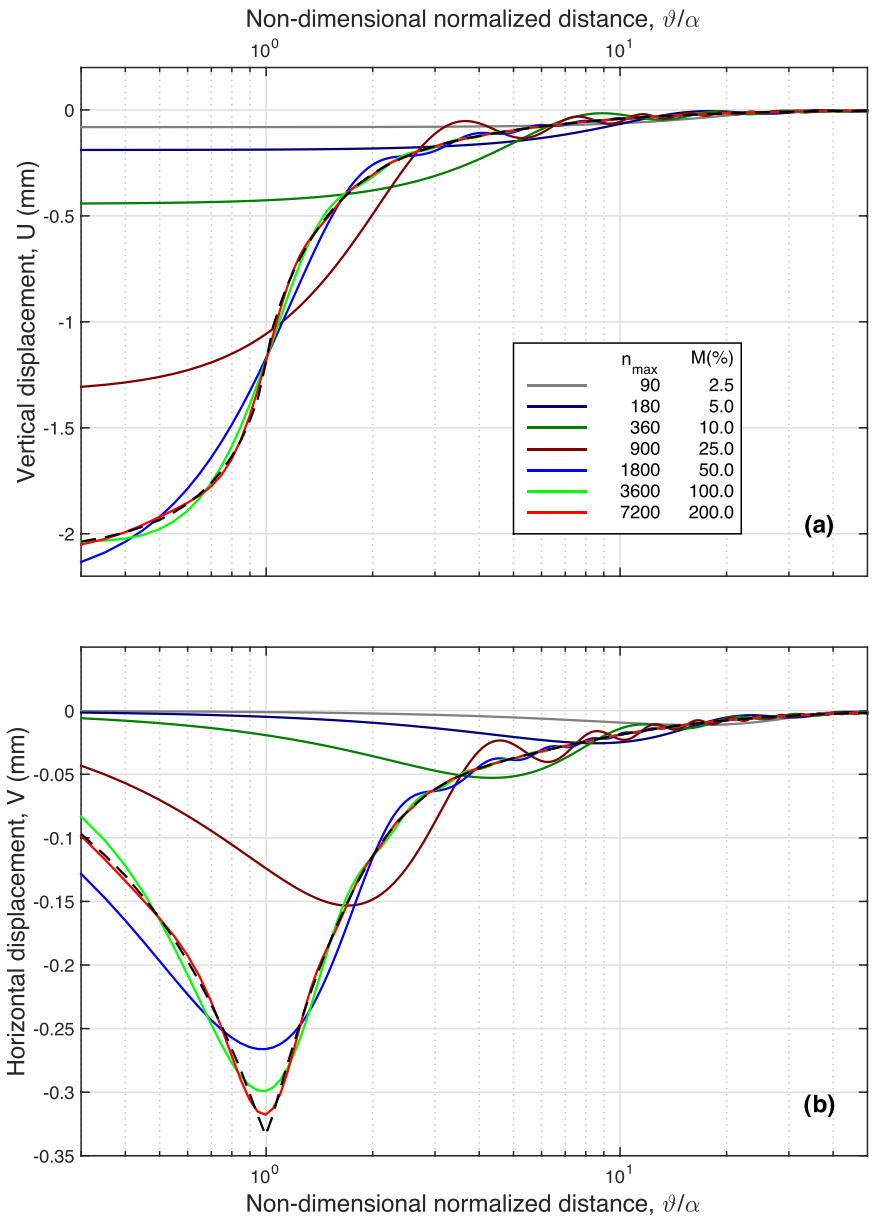

Figure 4. Surface displacements $U(\vartheta)$ (a) and $V(\vartheta)$ (b), obtained adopting a range of truncation degrees $n_{\max}$, varying from $n_{\max} = 2\,\overline{n}_{\max}$ (where $\overline{n}_{\max} = 3600$ corresponds to the ROT given by eq. 14) down to $n_{\max} = 90$. Here M represents the ratio $n_{\max}/\overline{n}_{\max}$, expressed as a percentage. The dashed curve, reproduced from Fig. 3, is for $n_{\max} = 40\,000$.

maturity of our expansions, M, to be $n_{\max}/\overline{n}_{\max}$. For all practical purposes, the solution obtained with $n_{\max} = 40\,000$ can be considered, for $\alpha = 0.1^\circ$, the true solution. From the results in Fig. 4, it is apparent that for $n_{\max} = \overline{n}_{\max} = 3600$ (light green curves) the 'true' solutions obtained using $n_{\max} = 40\,000$ (see dashed lines) are reasonably well reproduced. However, oscillations due to the deficiency of short-wavelength terms imposed by premature truncation of the Legendre expansions (10) and (12) are clearly visible in the whole range of ϑ values. Note that the extreme values $U(\vartheta = 0)$ and $V(\vartheta = \alpha)$ are approximated well and fairly well, respectively. A value $n_{\max} = 2\,\overline{n}_{\max} = 7200$ (red curves) would basically reproduce the true solutions (this would suggest, for the ROT, the more conservative but more time consuming choice $\overline{n}_{\max} = 7200$). Overall, the displacements obtained using $n_{\max} = \overline{n}_{\max}/2 = 1800$ still bear a marked resemblance to the true displacements; however, decreasing $n_{\max}$ below this value produces a complete deterioration of the solutions.

To estimate quantitatively the error precipitated by premature truncation, we have computed numerically the non-dimensional misfit

$$\mathcal{E}_F(n_{\max}) = \frac{\displaystyle\int_0^\beta (F(\vartheta) - F_{\text{true}}(\vartheta))^2 \sin\vartheta \,\mathrm{d}\vartheta}{\displaystyle\int_0^\beta F_{\text{true}}^2(\vartheta) \sin\vartheta \,\mathrm{d}\vartheta}, \tag{15}$$

where $F(\vartheta)$ represents any of the functions $U(\vartheta)$, $V(\vartheta)$ or $G(\vartheta)$ expanded to degree $n_{\max}$, $F_{\text{true}}(\vartheta)$ is their value for $n_{\max} = 40\,000$ and here we have chosen $\beta = 50\,\alpha = 5^\circ$. The misfit, shown as a function of $n_{\max}$ in Fig. 5, is ≈ 1 for small $n_{\max}$ values, since in this case $F(\vartheta) \ll F_{\text{true}}(\vartheta)$ (see Fig. 4). With increasing $n_{\max}$, $\mathcal{E}_F(n_{\max})$

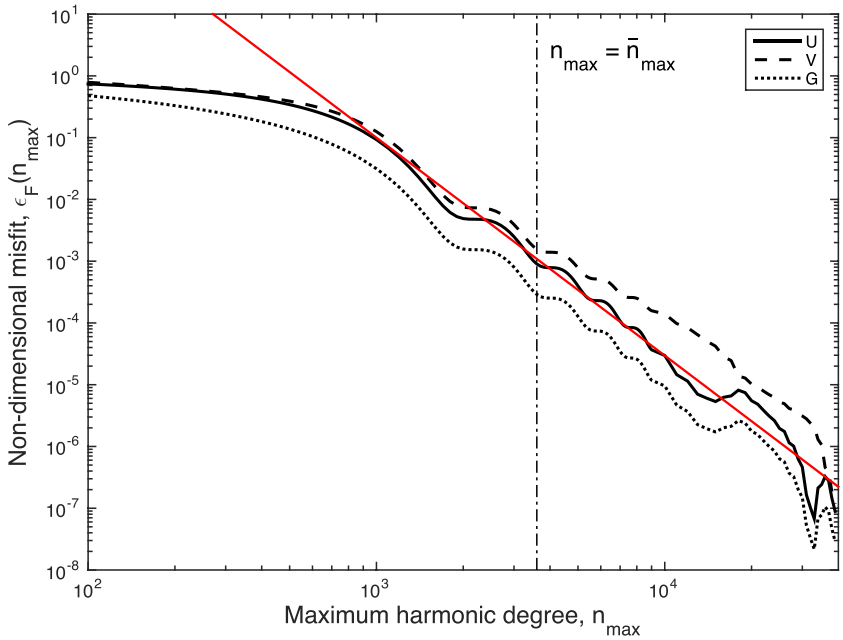

Figure 5. Misfit value $\mathcal{E}_F$, defined by eq. (16), as a function of the truncation degree $n_{\max}$, for $F(\vartheta) = U(\vartheta)$, $V(\vartheta)$ and $G(\vartheta)$ (see solid, dashed and dotted curves, respectively). The vertical segment shows the $\overline{n}_{\max}$ value. The red line shows the best-fitting linear relationship (16).

starts decreasing very quickly, approximately following a power law. By a simple linear regression, for the misfit $\mathcal{E}_U$ we find the relationship

$$\mathcal{E}_U(n_{\max}) = c_U\, n_{\max}^{-3.4}, \tag{16}$$

where c_U is a constant, which is approximately valid for $n_{\max} > 1000$. From Fig. 5, we note that the truncation degree $n_{\max}$ required to obtain a given misfit level for $G(\vartheta)$ is systematically lower than for $U(\vartheta)$, while that for $V(\vartheta)$ always exceeds it. In the Supporting Information Text S2, eq. (16) is extended to values of α in the range $0.001^\circ \leq \alpha \leq 1^\circ$.

5 CONCLUSIONS

We have shown that one can normally compute the geoelastic response to a disk load with acceptable accuracy by setting the spectral truncation degree $n_{\max} = \overline{n}_{\max}$, as defined in the eq. (14), which constitutes our ROT. In the event that the station of interest is located right at the edge of the disk, and one is particularly interested in the vertical component of displacement, it would be reasonable to set $n_{\max} = 2\,\overline{n}_{\max}$ instead. However, while $\overline{n}_{\max} = 3600$ for a disk with a 0.1° radius, $\overline{n}_{\max}$ raises to 36 000 or 360 000 if the disk radius is reduced to 0.01° or 0.001°, something that is becoming a practical possibility given the increasing availability of ultra-high-resolution DEMs for the Antarctic and Greenland ice sheets and for many smaller ice fields and ice caps in other parts of the world. Computing the geoelastic response with very large values for $n_{\max}$ naturally rises concern because (i) the analyst may not be able to find lists of Love numbers that extend to very high degrees, and (ii) even if he or she could, there is some anxiety about how numerical round-off might have affected the computation of these Love numbers and/or any computations that utilize them. Since the amplitudes of the errors associated with premature truncation diminish quite rapidly with increasing distance from the disk, and because we normally model a distributed load (or load change) with a great many disks, very few of which have any stations in their near-field or even medium-field, the idea of judiciously and safely violating the ROT (14) becomes increasingly attractive. The best approach for doing this is to compute the total elastic response at each station due to all disks using multiple values for $n_{\max}$, so that the sensitivity to $n_{\max}$ can be carefully assessed. As we explain in the Supporting Information annex, our function `diskload` provides an efficient mechanism for doing this.

ACKNOWLEDGEMENTS

The figures have been drawn using the Generic Mapping Tools (GMT) of Wessel & Smith (1998). MB was supported by National Science Foundation (NSF) grant ARC-1111882. GS is funded by Programma Nazionale di Ricerche in Antartide (PNRA) 2013/B2.06 (CUP D32I14000230005). We thank Gaia Galassi for discussion and Pascal Gegout for providing the load Love numbers for the seismological model REF of Kustowski *et al.* (2007).

REFERENCES

Alfrey, T., 1944. Non-homogeneous stresses in viscoelastic media, *Q. Appl. Math.,* **2**(2), 113–119.

Becker, J.M. & Bevis, M., 2004. Love's problem, *Geophys. J. Int.,* **156**(2), 171–178.

Bevis, M., Kendrick, E., Cser, A. & Smalley, R., 2004. Geodetic measurement of the local elastic response to the changing mass of water in Lago Laja, Chile, *Phys. Earth planet. Inter.,* **141**(2), 71–78.

Bevis, M., Alsdorf, D., Kendrick, E., Fortes, L.P., Forsberg, B., Smalley, R. & Becker, J., 2005. Seasonal fluctuations in the mass of the Amazon River system and Earth's elastic response, *Geophys. Res. Lett.,* **32**(16), L16308, doi:10.1029/2005GL023491.

Bevis, M. *et al.*, 2012. Bedrock displacements in Greenland manifest ice mass variations, climate cycles and climate change, *Proc. Natl. Acad. Sci. USA,* **109**(30), 11 944–11 948.

Blewitt, G., Lavallée, D., Clarke, P. & Nurutdinov, K., 2001. A new global mode of Earth deformation: Seasonal cycle detected, *Science,* **294**(5550), 2342–2345.

Borsa, A., Moholdt, G., Fricker, H. & Brunt, K., 2014. A range correction for ICESat and its potential impact on ice-sheet mass balance studies, *The Cryosphere,* **8**(2), 345–357.

Boussinesq, J., 1885. *Applications of Potentials for the Study of Equilibrium and Movement of Elastic Solids,* Gautier-Villars.

Cathles, L., 1975. *The Viscosity of the Earth's Mantle,* Princeton Univ. Press.

Dahlen, F. & Tromp, J., 1998. *Theoretical Global Seismology,* Princeton Univ. Press.

Dong, D., Fang, P., Bock, Y., Cheng, M. & Miyazaki, S., 2002. Anatomy of apparent seasonal variations from GPS-derived site position time series, *J. geophys. Res.,* **107**(B4), ETG 9-1–ETG 9-16.

Farrell, W., 1972. Deformation of the Earth by surface loads, *Rev. geophys.,* **10**(3), 761–797.

Fu, Y., Argus, D.F., Freymueller, J.T. & Heflin, M.B., 2013. Horizontal motion in elastic response to seasonal loading of rain water in the Amazon Basin and monsoon water in Southeast Asia observed by GPS and inferred from GRACE, *Geophys. Res. Lett.,* **40**(23), 6048–6053.

Grapenthin, R., 2014. CRUSDE: A plug-in based simulation framework for composable CRUstal DEformation studies using Green's functions, *Comput. Geosci.,* **62,** 168–177.

Haskell, N., 1935. The motion of a viscous fluid under a surface load, *J. Appl. Phys.,* **6**(8), 265–269.

Heki, K., 2001. Seasonal modulation of interseismic strain buildup in northeastern Japan driven by snow loads, *Science,* **293**(5527), 89–92.

Jeans, J., 1923. The propagation of earthquake waves, *Proc. R. Soc. A,* **102,** 554–574.

Khan, S.A., Wahr, J., Bevis, M., Velicogna, I. & Kendrick, E., 2010. Spread of ice mass loss into northwest Greenland observed by GRACE and GPS, *Geophys. Res. Lett.,* **37**(6), L06501, doi:10.1029/2010GL042460.

Kustowski, B., Dziewoński, A.M. & Ekström, G., 2007. Nonlinear crustal corrections for normal-mode seismograms, *Bull. seism. Soc. Am.,* **97**(5), 1756–1762.

Lamb, H., 1901. On Boussinesq's problem, *Proc. Lond. Math. Soc.,* **1**(1), 276–284.

Lee, G.H., 1950. *An Introduction to Experimental Stress Analysis,* Wiley.

Longman, I., 1962. A Green's function for determining the deformation of the Earth under surface mass loads: 1. Theory, *J. geophys. Res.,* **67**(2), 845–850.

Longman, I., 1963. A Green's function for determining the deformation of the Earth under surface mass loads. 2. Computations and numerical results, *J. geophys. Res.,* **68,** 485–496.

Love, A.E.H., 1911. *Some Problems of Geodynamics: Being an Essay to which the Adams Prize in the University of Cambridge was Adjudged in 1911,* CUP Archive.

Love, A.E.H., 1929. The stress produced in a semi-infinite solid by pressure on part of the boundary, *Phil. Trans. R. Soc. Lond., A,* **228,** 377–420.

Mangiarotti, S., Cazenave, A., Soudarin, L. & Cretaux, J., 2001. Annual vertical crustal motions predicted from surface mass redistribution and observed by space geodesy, *J. geophys. Res.,* **106**(B3), 4277–4291.

Melini, D., Gegout, P., King, M., Marzeion, B. & Spada, G., 2015a. On the rebound: Modeling Earth's ever-changing shape, *EOS, Trans. Am. geophys. Un.,* **96,** doi:10.1029/2015EO033387.

Melini, D., Gegout, P., Spada, G. & King, M., 2015b. - *a Regional ElAstic Rebound calculator - User Manual for version 1.0.*', Available at: http://danielemelini.github.io/rear/, last accessed 1 April 2016.

Munk, W.H. & MacDonald, G.J., 1960. *The Rotation of the Earth: A Geophysical Discussion,* Cambridge Univ. Press.

Na, S.-H. & Baek, J., 2011. Computation of the load Love number and the load Green's function for an elastic and spherically symmetric earth, *J. Korean Phys. Soc.,* **58**(5), 1195–1205.

Nielsen, K., Khan, S.A., Korsgaard, N.J., Kjær, K.H., Wahr, J., Bevis, M., Stearns, L.A. & Timm, L.H., 2012. Crustal uplift due to ice mass variability on Upernavik Isstrøm, west Greenland, *Earth planet. Sci. Lett.,* **353,** 182–189.

Nielsen, K., Khan, S.A., Spada, G., Wahr, J., Bevis, M., Liu, L. & Dam, T., 2013. Vertical and horizontal surface displacements near Jakobshavn Isbræ driven by melt-induced and dynamic ice loss, *J. geophys. Res.,* **118**(4), 1837–1844.

Pan, E., Bevis, M., Han, F., Zhou, H. & Zhu, R., 2007. Surface deformation due to loading of a layered elastic half-space: a rapid numerical kernel based on a circular loading element, *Geophys. J. Int.,* **171**(1), 11–24.

Pan, E., Chen, J., Bevis, M., Bordoni, A., Barletta, V. & Molavi Tabrizi, A., 2015. An analytical solution for the elastic response to surface loads imposed on a layered, transversely isotropic and self-gravitating Earth, *Geophys. J. Int.,* **203,** 2150–2181.

Peltier, W. & Andrews, J., 1976. Glacial-isostatic adjustment – I. The forward problem, *Geophys. J. Int.,* **46**(3), 605–646.

Press, W.H., 2007. *Numerical Recipes: The Art of Scientific Computing,* 3rd edn, Cambridge Univ. Press.

Read, W., Jr., 1950. Stress analysis for compressible viscoelastic materials, *J. Appl. Phys.,* **21**(7), 671–674.

Shida, T., 1912. *On the Elasticity of the Earth and the Earth's Crust,* Kyoto Imperial University.

Spada, G., 1993. *The Theory behind TABOO,* Samizdat Press.

Spada, G., 2008. ALMA, a Fortran program for computing the viscoelastic Love numbers of a spherically symmetric planet, *Comput. Geosci.,* **34**(6), 667–687.

Spada, G. *et al.*, 2011. A benchmark study for glacial isostatic adjustment codes, *Geophys. J. Int.,* **185**(1), 106–132.

Spada, G., Ruggieri, G., Sørensen, L.S., Nielsen, K., Melini, D. & Colleoni, F., 2012. Greenland uplift and regional sea level changes from ICESat observations and GIA modelling, *Geophys. J. Int.,* **189**(3), 1457–1474.

Steckler, M.S., Nooner, S.L., Akhter, S.H., Chowdhury, S.K., Bettadpur, S., Seeber, L. & Kogan, M.G., 2010. Modeling Earth deformation from monsoonal flooding in Bangladesh using hydrographic, GPS, and Gravity Recovery and Climate Experiment (GRACE) data, *J. geophys. Res.,* **115**(B8), doi:10.1029/2009JB007018.

Terazawa, K., 1916. On the elastic equilibrium of a semi-infinite solid under given boundary conditions, with some applications, *J. Coll. Sci. Imperial Univ. Tokyo,* **37**(7), 1–64.

Vandam, T.M., Blewitt, G. & Heflin, M.B., 1994. Atmospheric pressure loading effects on Global Positioning System coordinate determinations, *J. geophys. Res.,* **99**(B12), 23 939–23 950.

Wessel, P. & Smith, W.H.F., 1998. New, improved version of Generic Mapping Tools released, *EOS, Trans. Am. geophys. Un.,* **79**(47), 579, doi: 10.1029/98EO00426.

Wu, P. & Peltier, W., 1982. Viscous gravitational relaxation, *Geophys. J. Int.,* **70**(2), 435–485.

SUPPORTING INFORMATION

Additional Supporting Information may be found in the online version of this paper:

Figure S1. Vertical (U), horizontal (V) displacement and geoid change (G) for a disk load with $\alpha = 0.1^\circ$ and load thickness $T_w = +1$ m, as a function of normalized colatitude ϑ/α, computed with $n_{\min} = 0$ and $n_{\max} = 40\,000$.

Figure S2. Vertical (U), horizontal (V) displacement and geoid change (G) for a disk load with $\alpha = 0.1^\circ$ and load thickness $T_w = +1$ m, computed at a colatitude $\vartheta = 1.5\ \alpha$ as a function of the maximum degree $n_{\max}$. The U component oscillates to larger $n_{\max}$ than V and G since h_n reaches a constant amplitude with increasing n while l_n and k_n decay as n^{-1}, thus stabilizing faster (see main text). Horizontal dashed lines represent the 'true' values computed at $n_{\max} = 40\,000$; vertical dash-dotted lines mark the 'rule of thumb' $\bar{n}_{\max} = 3\,600$, and the 'safer rule of thumb' $\bar{n}_{\max} = 7\,200$, according to eq. (14).

Figure S3. Non-dimensional misfit ε_U as a function of disk radius α and truncation point $n_{\max}$ (blue contours) and its linear regression model according to eq. (S1) (red contours). The green dashed line represents the 'rule of thumb' $\bar{n}_{\max} = 360^\circ/\alpha$.

Figure S4. 3D view of the non-dimensional misfit ε_U as a function of disk radius α and truncation point $n_{\max}$. The wire-frame plane represents the error regression model of eq. (S1).

Figure S5. Misfit value ε_F as a function of the truncation degree $n_{\max}$ for various disk sizes α. The vertical segments mark the $\bar{n}_{max}$ value defined in eq. (14); the red line corresponds to the global approximation presented in eq. (S1).

Figure S6. (a) Normalized surface displacements for various values of α, (b) Maximum values of surface displacements with varying α. Dashed lines show a linear scaling. In both frames, $T_w = +1$ m.

Table S1. Contents of the `diskload.zip` archive.

(http://gji.oxfordjournals.org/lookup/suppl/doi:10.1093/gji/ggw115/-/DC1).

Please note: Oxford University Press is not responsible for the content or functionality of any supporting materials supplied by the authors. Any queries (other than missing material) should be directed to the corresponding author for the paper.